Chemical Engineering Communications
Publication details, including instructions for authors and subscription information:
http://www.informaworld.com/smpp/title~content=t713454788

CLUSTER KINETICS OF PHASE TRANSITIONS: APPLICATIONS TO INNOVATIVE TECHNOLOGIES

Benjamin J. McCoy [a]; Giridhar Madras [b]
[a] Department of Chemical Engineering and Materials Science, University of California, Davis, California, USA
[b] Department of Chemical Engineering, Indian Institute of Science, Bangalore, India

Online Publication Date: 01 January 2009

To cite this Article McCoy, Benjamin J. and Madras, Giridhar(2009)'CLUSTER KINETICS OF PHASE TRANSITIONS: APPLICATIONS TO INNOVATIVE TECHNOLOGIES',Chemical Engineering Communications,196:1,204 — 233
To link to this Article: DOI: 10.1080/00986440802290094
URL: http://dx.doi.org/10.1080/00986440802290094

Chem. Eng. Comm., 196:204–233, 2008

ISSN: 0098-6445 print/1563-5201 online
DOI: 10.1080/00986440802290094

Taylor & Francis
Taylor & Francis Group

Cluster Kinetics of Phase Transitions: Applications to Innovative Technologies

BENJAMIN J. McCOY[1] AND GIRIDHAR MADRAS[2]

[1]Department of Chemical Engineering and Materials Science, University of California, Davis, California, USA
[2]Department of Chemical Engineering, Indian Institute of Science, Bangalore, India

Phase transitions are critical in many of the new technologies of interest to chemical engineers. Applications to materials processing and pharmaceuticals manufacture are among the uses for phase transition dynamics investigated with the methods of population balance modeling for clustering processes. The underlying phenomenon of clustering occurs during condensation processes such as crystallization from solution. Self-assembly of molecules or supramolecules is likewise spontaneous clustering, often through non-covalent interactions. Vapor-liquid and solid–liquid condensations usually involve nucleation from a metastable state, accompanied by particulate growth and Ostwald ripening (with denucleation). The nucleation process is bypassed under certain conditions, such as in spinodal decomposition, glass transition, and gelation. It is proposed that the unifying concept for all these transformations is cluster kinetics and dynamics. Using population balance modeling, we outline how phase transition processes can be quantitatively modeled by cluster size distributions evolving in time. We also discuss how generic cluster processes apply to granular systems, synchronizing oscillators, and polymorphic transformations.

Keywords Continuous distribution kinetics; Crystal growth; Nucleation; Ostwald ripening; Phase transitions; Population balance equations

Introduction

Population balance modeling (PBM) has been applied to a wide range of processes, including liquid-liquid and gas-liquid dispersions, particle fragmentation and agglomeration, crystallization and crystal growth, hydrocarbon cracking and polymer degradation (free radical mechanisms), polymerization (chain and step), cell growth and fission, cell aggregation and deaggregation, and clustering phenomena. An attractive feature of PBM is that the concepts and equations are similar, except for the specific forms of the aggregation and fragmentation kernels or rate coefficient expressions that may apply. As the methodology always involves distributions (of molecular weights, particle mass, number of polymeric branches, crystal length, or other property), we have referred to the approach as "distribution kinetics and dynamics." PBM has evolved to constitute a powerful tool for solving problems with distributions of particles or macromolecules. Four central processes in the mechanisms for these processes

Address correspondence to Benjamin J. McCoy, Department of Chemical Engineering and Materials Science, University of California, Davis, CA 95616, USA. E-mail: bjmccoy@ucdavis.edu

are: (1) aggregation, (2) fragmentation, (3) monomer addition, and (4) monomer removal from a cluster. Considered separately or in combination, these processes allow analysis of a multitude of natural and industrial phenomena.

The classical models of phase transitions are by Becker and Doring (BD) (1935), Lifshitz and Slyozov (LS) (1961) and Wagner (W) (1961). The BD model for condensation from the metastable state was based on the formation of clusters by the addition or subtraction of monomers (with no coalescence among larger clusters). The BD equations were generalized (Penrose and Lebowitz, 1976) to allow the monomer concentrations to vary, with the constraint that only monomers can interact with clusters. The LSW theory is concerned with ripening (coarsening) of the cluster size distribution due to transfer of mass from smaller, less stable clusters to larger, more stable clusters, with attendant dissolution of unstable (subcritical) clusters. Marqusee and Ross (1983) showed that the LSW solution represents terms in an expansion of the long time solution. More recent studies of the BD and LSW equations explain the connections between them (Laurençot and Mischler, 2002) and the observed time regimes (Bolton and Wattis, 2002).

Crystallization, in its full generality, involves nucleation, crystal growth, and Ostwald ripening. The cluster kinetics approach explains the behavior observed for polymer crystallization, important to plastics processing. The cluster kinetics approach also describes non-nucleated processes, such as glass transition behavior: how rapidly cooling or compressing a liquid or colloid leads to structural arrest of molecular motion and a consequent sharp rise in viscosity or dielectric relaxation time. According to transition state theory, activation energies or volumes are used for varying temperature or pressure processes, respectively, in the rate coefficients for monomer-cluster addition-dissociation and cluster aggregation-breakage. The model leads to scaled temperature and pressure correlations for viscosity (or dielectric relaxation time) that reveal strong and fragile glass behavior and agree with experimental data. Spinodal decomposition (barrierless phase transition) is a spontaneous, unnucleated phase separation caused by conditions that force the system to become thermodynamically unstable. The PBM approach predicts the two time regimes observed experimentally.

The objective of this article is to review and summarize some of the advances in applying cluster kinetics and dynamics to phase transition phenomena important to developments on the frontiers of modern chemical engineering. We begin with crystallization and its accompanying processes: ripening, agglomeration, breakage, attrition, and polymorphic transformations. We represent self-assembly as an aggregation process closely related to crystallization. We show how non-nucleated phenomena such as spinodal decomposition, gelation, glass transition, and oscillator synchronization are related to the basic clustering mechanisms.

Crystallization with Agglomeration and Breakage

For crystallization, combined aggregation and monomer addition (growth) is often called agglomeration. The reverse is dissolution (monomer removal) and breakage. Solution concentration, either supersaturated or undersaturated, drives the reversible growth or dissolution, respectively. The relative saturation, or degree of nonequilibrium, is determined by thermodynamics, principally the Gibbs-Thomson relationship for interfacial energy. Smaller particles have a higher fugacity and are more soluble. Larger particles are less soluble and thus tend to grow at the expense

of smaller particles, leading to Ostwald ripening. Crystallization occurs from the metastable, supersaturated state into a particular crystal structure. The three basic processes in condensation phase transition are nucleation, growth, and ripening (Marqusee and Ross, 1983). These processes are not sharply distinguished, but in fact overlap during the evolution from a supersaturated phase to a single condensed ripened particle in equilibrium with the non-condensed phase. The current work uses distribution kinetics to describe the complete time range for transition from a homogeneous supersaturated phase through the first appearance of nuclei, subsequent monomer deposition and growth, and eventual ripening to a single large remaining cluster.

We are guided by distribution kinetics, previously applied to polymerization-degradation processes (McCoy and Madras, 1997; Madras and McCoy, 1998, 2001), in formulating reversible growth and aggregation-fragmentation processes for crystals. Let x and x_m be the molecular weights of crystals and monomer, respectively. For a spherical particle the particle mass x is related to the crystal mass density ρ_c and particle radius r by $x = (4/3)\pi r^3 \rho_c$. A general representation of reversible addition of monomer, $\mathbf{M}(x_m)$, to a crystal, $\mathbf{C}(x)$, can be written as

$$\mathbf{C}(x) + \mathbf{M}(x_m) \underset{k_d(x)}{\overset{k_g(x)}{\rightleftarrows}} \mathbf{C}(x + x_m) \tag{1}$$

with growth and dissolution rate coefficients, respectively, denoted by k_g and k_d. The crystals may aggregate with rate coefficient k_a or fragment with breakage rate coefficient k_b:

$$\mathbf{C}(x) + \mathbf{C}(x') \underset{k_b(x)}{\overset{k_a(x)}{\rightleftarrows}} \mathbf{C}(x + x') \tag{2}$$

In general, all four rate coefficients are functions of x, which has a significant influence on the system dynamics.

The population balance equations that govern the distribution of the crystals, c(x, t), and of the monomer, $m(x,\ t) = m^{(0)}(t)\delta(x - x_m)$, are based on mass conservation for the processes of Equations (1) and (2):

$$\begin{aligned}\partial c(x,t)/\partial t = &-k_g(x)c(x,t)\int_o^\infty m(x',t)dx' + \int_o^x k_g(x-x')c(x-x',t)m(x',t)dx' \\ &- k_d(x)c(x,t) + \int_x^\infty k_d(x')c(x',t)\delta(x-(x'-x_m))dx' \\ &- 2k_a c(x,t)\int_o^\infty c(x',t)dx' + k_a\int_o^x c(x',t)c(x-x',t)dx' \\ &- k_b(x)c(x,t) + 2\int_x^\infty k_b(x')c(x',t)dx'/x' - I\delta(x-x^*)\end{aligned} \tag{3}$$

and

$$\begin{aligned}\partial m(x,t)/\partial t = &-m(x,t)\int_o^\infty k_g(x')c(x',t)dx' + \int_x^\infty k_d(x')c(x',t)\delta(x-x_m)dx' \\ &+ I\delta(x-x^*)x^*/x_m\end{aligned} \tag{4}$$

Nucleation of crystals of mass x^* at rate I is a source term or, in case of ripening, a sink term for denucleation, which occurs when crystals shrink to their critical size, x^*, and then spontaneously vanish. We thus distinguish between ordinary dissolution due to concentration driving forces and total disintegration due to thermodynamic instability.

Rate Coefficients

Diffusion- and surface-controlled growth can be expressed in terms of particle mass x:

$$k_g(x) = \kappa_g x^{\lambda} \tag{5}$$

where $\lambda = 1/3$ represents diffusion-controlled growth. When growth is limited by monomer deposition and dissociation at the particle surface (Xia and Zinke-Allmang, 1998), the rate coefficient is proportional to the particle surface area so that $\lambda = 2/3$. If the deposition is independent of the surface area, then $\lambda = 0$. Other values of λ may be realistic for other rate processes (Olson and Hamill, 1996; Bhakta and Ruckenstein, 1995). The breakage rate coefficient typically increases with increased particle mass, $k_b(x) = \kappa_b x^{\nu}$, and for $\nu = 1$, an exact similarity solution is obtained when breakage alone occurs. When aggregation is not a primary issue, the aggregation rate coefficient, k_a, is considered constant (independent of mass). Microscopic reversibility (detailed balance) (Reif, 1965; De Groot and Mazur, 1962) allows the calculation of $k_d(x)$, given an expression for $k_g(x)$:

$$k_d(x) = m_{eq}^{(0)}\, k_g(x) \tag{6}$$

For a spherical cluster the local-equilibrium interfacial concentration at the cluster surface is given by the Gibbs-Thomson equation in terms of the solubility of a flat surface, $m_{\infty}^{(0)}$:

$$m_{eq}^{(0)} = m_{\infty}^{(0)} \exp(\Omega) \tag{7}$$

where

$$\Omega = 2\sigma x_m / r_c \rho_c RT \tag{7a}$$

in terms of monomer molar volume $v = x_m/\rho_c$, interfacial energy σ, the gas constant R, and absolute temperature T. To establish an expression for the dissolution rate coefficient, we substitute the Gibbs-Thomson equation into Equation (6) to get

$$k_d(x) = \kappa_d x^{\lambda} \exp[\omega/(x/x_m)^{1/3}] \tag{8}$$

where $\kappa_d = \kappa_g m_{\infty}^{(0)}$ and $\omega = (4\pi x_m^2/3\rho_c^2)^{1/3} 2\sigma/k_B T$, the ratio of monomer interfacial energy to thermal energy, which plays a key role in controlling nucleation, growth, and ripening (denucleation).

The governing PBEs, Equations (3) and (4), can be made dimensionless by defining the scaled quantities to minimize the number of parameters and simplify the numerical analysis (Madras and McCoy, 2002):

$$\xi = x/x_m,\ \theta = t\kappa_g m_{\infty}^{(0)} x_m^{\lambda},\ S = m^{(0)}/m_{\infty}^{(0)},\ C = c x_m/m_{\infty}^{(0)},\ C^{(n)} = c^{(n)}/(m_{\infty}^{(0)} x_m^{n}),$$
$$J = I/(\kappa_g m_{\infty}^{(0)2} x_m^{\lambda}),\ \psi_a = k_a/(\kappa_g x_m^{\lambda}),\ \psi_b = \kappa_b/(\kappa_g m_{\infty}^{(0)} x_m^{\lambda-\nu}) \tag{9}$$

The mass balance, based on moments of Equations (3) and (4), is always satisfied, thus:

$$S(\theta) = S_o + C_o^{(1)} - C^{(1)}(\theta) \tag{10}$$

and can be substituted into the PBE to give the dimensionless equation for C:

$$\begin{aligned}\partial C(\xi,\theta)/\partial\theta = {} & [S_o + C_o^{(1)} - C^{(1)}(\theta)][-\xi^{\lambda}C(\xi,\theta) + (\xi-1)^{\lambda}C(\xi-1,\theta)] \\ & - \xi^{\lambda}\exp(\omega\xi^{-1/3})C(\xi,\theta) + (\xi+1)^{\lambda}\exp(\omega(\xi+1)^{-1/3})C(\xi+1,\theta)] \\ & - 2\psi_a C(\xi,\theta)C^{(0)}(\theta) + \psi_a\int_o^{\xi} C(\xi',\theta)C(\xi-\xi',\theta)d\xi' \\ & - \psi_b\xi^{\nu}C(\xi,\theta) + 2\psi_b\int_{\xi}^{\infty}\xi'^{\nu}C(\xi')d\xi'/\xi' - J\delta(\xi-\xi^*)\end{aligned} \tag{11}$$

Nucleation

The nucleation rate expression is given by (Debenedetti, 1996)

$$J = \alpha S^2\exp[-\omega^3/2(\ln S)^2] \tag{12}$$

where $\alpha = (2\sigma x_m^{1-2\lambda}N_A/\pi\gamma^2\rho_c)^{1/2}$. The relationship of interfacial to thermal energy gives the Gibbs-Thomson expressions:

$$\Omega(\xi) = \omega/\xi^{1/3} \quad \text{and} \quad \xi^* = (\omega/\ln S)^3 \tag{13}$$

The cluster mass, ξ, is scaled in units of monomer mass, x_m, and hence equals the number of monomers in a cluster. The Gibbs-Thomson relation applies to each cluster in Equation (13) so that Ω is a function of ξ and larger clusters grow while smaller clusters dissolve.

Denucleation

A key difference from previous ripening theories is our treatment of denucleation. In accordance with classical nucleation theory (Debenedetti, 1996), we consider that clusters of a size less than the critical nucleus size are unstable and exist only as short-lived fluctuations. Such unstable clusters, having only a transitory existence, are assumed to disintegrate instantaneously and spontaneously into the monomer phase. Whereas other approaches (Zinke-Allmang, 1997) consider that all cluster sizes down to zero mass exist in the crystal size distribution, we require that clusters smaller than the thermodynamically stable size will dissolve spontaneously. This provides a rational and predictable way to reduce the cluster population until only one large particle exists at $t \to \infty$, as dictated by Ostwald ripening. Assuming denucleation to be instantaneous for unstable clusters is an obvious approximation. Because cluster growth and shrinkage control Ostwald ripening as the slowest and therefore rate-determining processes, the approximation is deemed reasonable.

Conventional models based on a size-independent agglomeration kernel without fragmentation will not predict a steady state because the size would continuously increase with time. The current model shows that the average crystal size reaches steady state, even when aggregation does not occur. When agglomeration occurs,

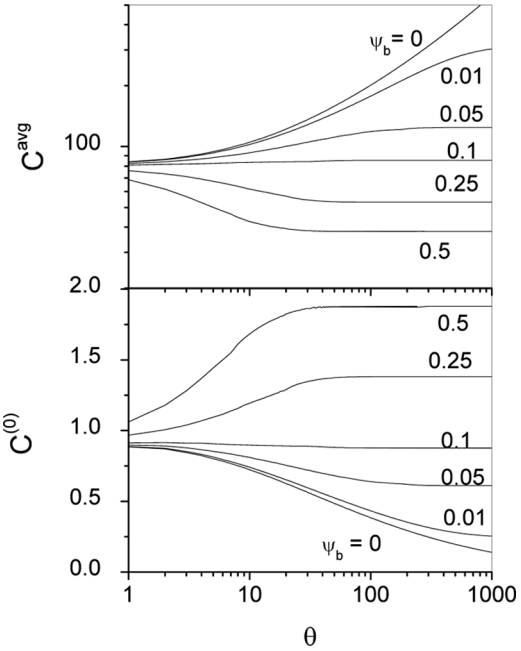

Figure 1. Effect of the breakage parameter ψ_b on the time evolution of particle number concentration $C^{(0)}$ and particle average mass C^{avg} for $\psi_a = 0$. The parameters in the calculations are $S_o = \omega = 5$, $C_o^{(0)} = 1$, $\lambda = 0$, and $\nu = 0$. The initial distribution is an exponential distribution given with $C_o^{avg} = 75$.

a steady state obtains when the denucleation rate equals the rates of fragmentation and agglomeration. Figure 1 shows the time evolution of the crystal number concentration and average crystal size for a fragmentation kernel with $\nu = 0$ in the absence of agglomeration ($\psi_a = 0$). For $\psi_b > 0$ the number concentration and average crystal size reach steady state, whereas for $\psi_b = 0$, Ostwald ripening causes the crystal size distribution to evolve over a very long time to a single large particle. The steady state implies that denucleation caused by breakage into subcritical clusters is balanced by growth and not necessarily by aggregation.

Attrition

During the operation of crystallizers, attrition can occur by impacts between the suspended solids, the moving and nonmoving parts of the equipment, and the crystals themselves. When agitation energy is low, an elastic deformation of the crystal may occur, and, as the impact energy increases, the resistance of some regions on the crystal surface is overcome, causing abrasion fracture. When the resistance of the whole crystal is exceeded, the crystal shatters according to the fragmentation mechanism. Attrition can occur by a fragmentation mechanism when the collision energy is sufficient to cause localized particle fracture, or by an abrasion mechanism when the collision energy is capable of removing only small amounts of material from the surface of the particle.

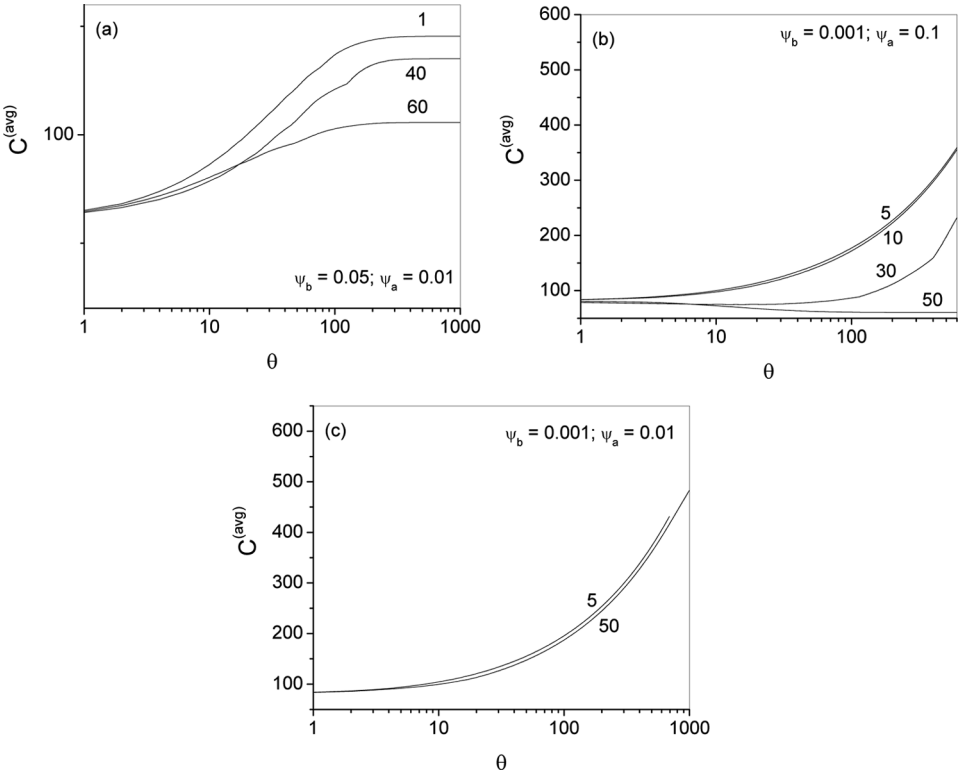

Figure 2. Effect of the attrition product particle of size ξ_i on the time evolution of the particle average size $C^{(avg)}$. The parameters in the calculations are $S_o = \omega = 5$, $C_o^{(0)} = 1$, $\lambda = 0$, and $\nu = 0$ with (a) $\psi_a = 0.01$ and $\psi_b = 0.05$, (b) $\psi_a = 0.001$ and $\psi_b = 0.1$, and (c) $\psi_a = 0.001$ and $\psi_b = 0.01$. The initial distribution is an exponential distribution with $C_o^{avg} = 75$.

Crystalline materials are prone to attrition owing to their inherent fragility and to the agitation required for homogeneity and transfer of heat and mass. The consequences of attrition are multifold: it reduces average particle size, changes the particle size distribution, and modifies particle morphology. The influence of operating conditions on attrition phenomena occurring during crystallization has been a topic of active research (Nienow and Conti, 1978; Ayazi Smalou et al., 1990; Ploss and Mersmann, 1989; Mazzarotta et al., 1993).

In the case of attrition, Equation (2) may be rewritten as

$$\mathbf{C}(x) \xrightarrow{k_b(x)} \mathbf{C}(x - x') + \mathbf{C}(x') \tag{2a}$$

$$\mathbf{C}(x) \xrightarrow{k_a(x)} \mathbf{C}(x - x_i) + \mathbf{C}(x_i) \tag{2b}$$

The small-particle product of attrition, $\mathbf{C}(x_i)$, has mass x_i, hence its distribution is a Dirac delta distribution. One can have many attrition product sizes represented as a sum of delta distributions. Figure 2 shows the variation of the average particle mass for different attrition product particle sizes ($\xi_i = x_i/x_m$) for various rates of fragmentation and attrition. Figure 2(a) represents the case when the rate of breakage is high. In this case, steady state is reached irrespective of attrition product particle size.

Figure 2(b) represents the case when the breakage rate is almost zero and the attrition rate is high. In this case, a steady-state value is reached only when the attrition product particle size has a size larger than the initial critical nucleus size, which can be very small, e.g., 30 molecules. When the attrition product particle size is smaller than the critical size, denucleation occurs and the average particle size continuously increases with time. Figure 2(c) represents the case when the rates of attrition and fragmentation are small. In this case, because Ostwald ripening dominates, the particle size continuously increases with time and steady state will never be attained. The present model therefore demonstrates that steady state may or may not be reached depending on the relative rates of fragmentation and attrition and the attrition product particle size. When the rates of both attrition and fragmentation are negligible, the size of the crystals grows continuously because Ostwald ripening dominates. A steady state in particle size is reached irrespective of the size of the attrition product particle when the fragmentation rate dominates. In case the rates of fragmentation and attrition are comparable, the evolution of the steady state depends on whether the size of the attrition product crystal is larger than the critical nucleus size. All this demonstrates the contributions of attrition and fragmentation and how, especially at later stages, Ostwald ripening influences the evolution of the crystal size distribution.

Polymer Crystallization

Understanding crystallization and melting in bulk polymers is a major issue in determining properties of polymeric materials. The central questions are different and more challenging than for crystallization of low molar mass systems. All the problems have technological relevance (Strobl, 2006) for control of mechanical properties for semicrystalline polymeric materials. In theoretical approaches dealing with the overall crystallization kinetics, an important issue is nucleation (Piorkowska et al., 2006).

A cluster size distribution approach for nucleation accompanied by crystal growth and Ostwald ripening serves to describe quantitatively the crystallization kinetics of polymer melt. Polymer nucleation and crystal growth involve the dynamics of polymer chains, including the folded chain structures. Population balance models based on crystal size distribution and concentration of amorphous polymer segments have been established. The related moment and governing differential equations can be solved numerically under isothermal and nonisothermal conditions (Yang et al., 2005a,b). The approach presents a fundamental explanation for the mechanism of nucleation and crystal growth. An outcome of the model is an explanation for the commonly observed Avrami plots for polymer crystallinity. The model was adapted to incorporate nonisothermal temperature procedures, cooling in particular, in polymer crystallization. Compared to the oversimplified Avrami theory, the approach yields a realistic explanation for Avrami plots by showing the curvature usually seen in experimental data. We have also extended this approach to the application of polymer blend crystallization (Yang et al., 2006a), in which the miscibility of polymer blends complicates the kinetics and dynamics of crystallization. This is important because the addition of one component affects the crystallization behavior of the other and can potentially be used to design and develop new types of high-performance polymer materials. Moreover, understanding

polymer crystallization behavior is needed to control product properties, e.g., microscopic structure, average size of polymer crystals, and crystal-size polydispersity.

A well-known description of crystallization kinetics is the phase transition concept of Avrami (1939), who adapted a metallurgical model to crystallization. The original derivations were simplified by Evans (1945) and rearranged for polymer crystallization by Meares (1965) and Hay (1971). The Avrami equation is given by

$$1 - X = e^{-Kt^n} \tag{14}$$

where X is the crystallinity and K is a constant. The exponent n depends not only on the structure of the crystal but also on the nature of nucleation (Avrami, 1940). Crystallization is the gradual building up of monomer on the nucleus surface in a melt or solution. A general representation of chain deposition on the crystal surface is same as Equation (1). Crystal breakage and aggregation are usually not considered in polymer crystallization, although such processes could be modeled similarly to particulate crystallization.

As the ratio of interfacial to thermal energy, ω influences nucleation and growth. By moment computations, the effects of ω are shown for 2-D and 3-D systems (Figure 3). The dotted lines represent 3-D while the solid lines represent the 2-D solution for a surface. The slope variation as ω changes is quite small in both 2-D and 3-D, and a larger slope is observed in the 2-D case. A small value of ω leads to a small critical size of crystal at constant supersaturation and finally leads to a large nucleation rate. Increasing ω delays nucleation and the decrease of supersaturation. Similar to the effect of the nucleation prefactor α, the influence of interfacial energy is notable only if ω is small; the slope difference disappears when ω is large. The explanation is that the crystal growth becomes the dominant term if ω is large, since the nucleation term exponentially decreases with ω^2. Comparing the numerical and the moment results reveals that the numerical result of crystallinity reaches an asymptotic value at large time while the moment result continues to increase. This is the influence of denucleation, which is ignored in the moment computations.

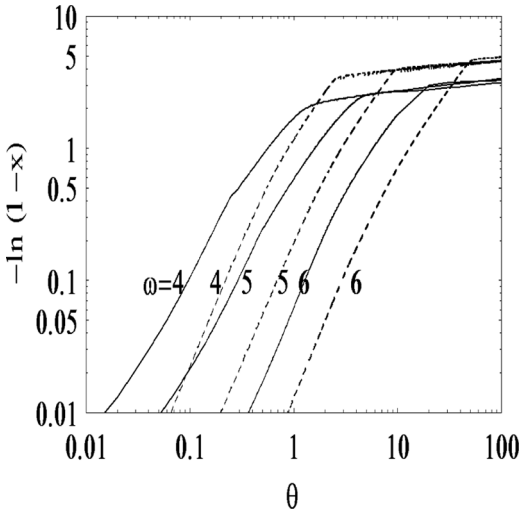

Figure 3. Comparison of polymer crystallinity plots by numerical solution for 2-D (dotted line) and 3-D (solid line) with $\lambda = 0$, $\alpha = 0.1$, and $S_0 = 50$.

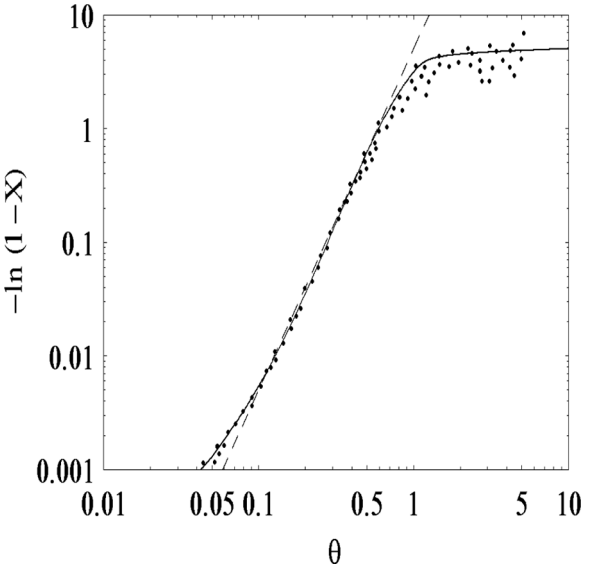

Figure 4. Comparison of the model to polypropylene crystallization experimental data; the solid line is a fit of the model and the dashed line is the Avrami equation with n = 3.0.

Figure 4 presents an Avrami plot for experimental polypropylene (PP) data at 110°C, showing the evolution of crystallinity X versus real time. The Avrami equation with n = 3.0 fits the data fairly well except where the data curve away from the Avrami equation at the end of crystallization. The solid line is our model prediction, and the predicted slope of 3.09 is close to the value of 3.0 reported by Ryan et al. (1999). It is interesting that the curve at the end of crystallization is predicted in the crystal size distribution model and fits the experimental data (Ryan et al., 1999) quite well. The Avrami equation, by contrast, provides a constant slope and thus fits only the intermediate data.

Polymorphic Crystallization

Some materials have more than one crystal structure; these different structures are called polymorphs. Molecules that have pharmacological activity are often quite complex and frequently take on polymorphic forms. The polymorphs may have different solubilities, different residence times in the body, and different therapeutic efficacies; hence, drugs are typically approved in only one polymorphic form. Maintaining the manufacturing facility free of unwanted crystalline seeds or heterogeneous nucleation templates is critical, as the polymorph that crystallizes depends strongly on how it nucleates. Polymorphs may also change with time, e.g., during processing or storage, motivating a concern for understanding polymorph transformations in depth. Polymorphs compete for substrate molecules in solution, causing one form to dominate over another.

Polymorph crystallization modeling requires an integration of thermodynamics, kinetics, reactor dynamics, population balances, and interfacial science. Cooling crystallization is a common method to prepare and separate polymorphs. It has been shown how two polymorphs (dimorphs) respond during cooling at different

concentrations when metastable zone limits and solubility curves (concentration versus temperature) cross. Elaborate procedures for controlling the rate of cooling or solvent evaporation during seeding have been recommended to manage polymorph production. Recent work by Yu (2003) indicates that classical concepts of crystallization are insufficient to describe polymorph nucleation phenomena. Cooling a crystal melt can nucleate a less stable polymorph on which a more stable polymorph can grow, and seeding with a particular polymorph can promote growth of another polymorph.

The deposition or condensation process by which monomers of mass $x' = x_m$ are reversibly added to or dissociated from a crystal can be represented by Equation (1). A process of solvent removal (e.g., by evaporation) with a time-dependent volume, V(t), is included in the accumulation terms.

The dimensionless equations for Equation (3) for polymorphs A and B are (Madras and McCoy, 2003)

$$\begin{aligned}[1/v(\theta)]\partial[v(\theta)C_A(\xi,\theta)]/\partial\theta = {} & S(\theta)\exp(-\varepsilon_A/\Theta)[-\xi^{\lambda}C_A(\xi,\theta) + (\xi-1)^{\lambda}C_A(\xi-1,\theta)] \\ & - \xi^{\lambda}\exp[-(h_A+\varepsilon_A)/\Theta]\exp[w_A(\Theta^{-1}-1)\xi^{-1/3}] \\ & \times C_A(\xi,\theta) + (\xi+1)^{\lambda}\exp[-(h_A+\varepsilon_A)/\Theta] \\ & \times \exp[w_A(\Theta^{-1}-1)(\xi+1)^{-1/3}]C_A(\xi+1,\theta) \\ & - J_A\delta(\xi-\xi_A^*) \end{aligned} \tag{3a}$$

and

$$\begin{aligned}[1/v(\theta)]\partial[v(\theta)C_B(\xi,\theta)]/\partial\theta = {} & S(\theta)\exp(-\varepsilon_B/\Theta)[-\xi^{\lambda}C_B(\xi,\theta) + (\xi-1)^{\lambda}C_B(\xi-1,\theta)] \\ & - \xi^{\lambda}\exp[-(h_B+\varepsilon_B)/\Theta]\exp[w_B(\Theta^{-1}-1)\xi^{-1/3}]C_B(\xi,\theta) \\ & + (\xi+1)^{\lambda}\exp[-(h_B+\varepsilon_B)/\Theta]\exp[w_B(\Theta^{-1}-1) \\ & \times (\xi+1)^{-1/3}]C_B(\xi+1,\theta) - J_B\delta(\xi-\xi_B^*) \end{aligned} \tag{3b}$$

The dimensionless equation for Equation (4) is

$$\begin{aligned}[1/v(\theta)]\partial[v(\theta)S(\theta)]/d\theta = {} & -S(\theta)[\exp(-\varepsilon_A/\Theta)C_A^{(\lambda)} + \exp(-\varepsilon_B/\Theta)C_B^{(\lambda)}] \\ & + \exp[-(h_A+\varepsilon_A)/\Theta]\exp[w_A(\Theta^{-1}-1)(C_A^{avg})^{-1/3}]C_A^{(\lambda)} \\ & + \exp[-(h_B+\varepsilon_B)/\Theta]\exp[w_B(\Theta^{-1}-1)(C_B^{avg})^{-1/3}]C_B^{(\lambda)}\Big\} \\ & + J_A\xi_A^* + J_B\xi_B^* \end{aligned} \tag{4a}$$

$C(\xi, \theta)$ represents the dimensionless cluster size distribution with the subscripts A and B denoting the two polymorphs, A and B. Supersaturation $S(\theta)$, temperature $\Theta(\theta)$, volume $v(\theta)$ are time-dependent variables common to the two polymorphs, while the independent variables are time θ and the number of monomers in the crystal ξ and are thus not subscripted. The ratio S is relative to the high temperature solubility μ_∞, which is assumed identical for polymorphs A and B. The other parameters are h ($=\Delta H/RT_c$), which is the dimensionless transition energy, ΔH, the molar energy of the phase transition, w, the Gibbs-Thomson ratio of interfacial to thermal energy for a cluster of monomer size, and $\varepsilon = E/RT_c$, the dimensionless activation energy where E is the activation energy for diffusion. These parameters are different for each polymorph and are subscripted. We describe the time evolution of the average size and mass of two polymorphs and show that interfacial and

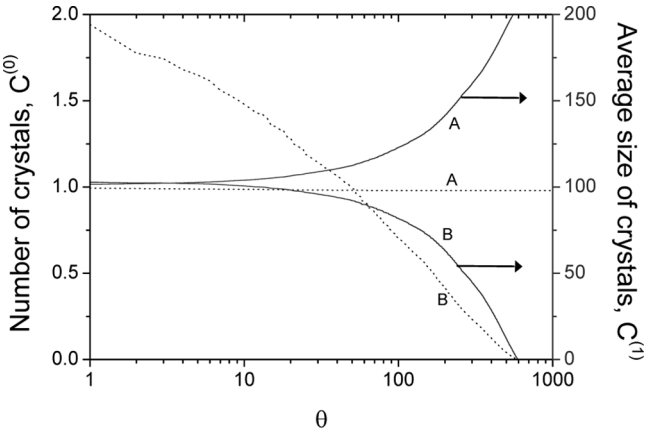

Figure 5. Evolution of the average size and number of polymorphic crystals A and B at temperature $\Theta = 0.5$ with $w_A = w_B = 1.0$, $\varepsilon_A = 0.01$, and $h_B = 0.75$, $h_A = 1.0$.

transition energies, but not activation energies, are significant in causing the less stable dimorph to vanish. The effect of transition energy (heat of crystallization) and thus solubility is shown in Figure 5. Smaller values of h imply higher solubility. In both Figures 2(a) and (b), $h_B < h_A$, so that B is more soluble than A. Again, the decline of B concentration is nearly proportional to log θ, eventually falling to zero. The computations corroborate the well-known principle that solubility is significant in determining polymorph separation. We have also shown how evaporative crystallization and cooling and heating programs are potential ways to control polymorph separation.

Self-Assembly

Already prevalent in natural biological systems (e.g., growth of bone, tooth enamel, cartilage), self-assembly is a promising method for design and production of nanostructures with specific chemical, electronic, or optical properties. The natural process of biomineralization yields intricately organized structures through self-assembly guided by templates and involving steps of nucleation, growth, and consolidation (Madras and McCoy, 2006). Surfactants self-assemble into spherical or cylindrical micelles that capture and carry guest components, a process that is the basis of detergency. Manufactured zeolites are engineered nanostructures with regular geometric patterns or pores that make them important in catalysis and separations. One way to drive self-assembly is to remove solvent so that the solutes become more concentrated such that the supersaturation is relieved by condensation (clustering) via intermolecular forces such as hydrogen bonding, van der Waals interactions, or electrostatic forces. The objective here is to describe the condensation phase transition with appropriate kinetics for the alignment and orientation mechanism. The model holds for 2-D and 3-D distributions, defined as c(x, t)dx, which represents the area of volume concentration of clusters at time t in the differential mass range (x, x + dx). Two processes are considered: the addition of monomer to a cluster, Equation (1), and the forward reaction for Equation (2). The mass balance equations, Equations (3) and (4), governing the crystal distribution, c(x, t), and

the monomer distribution, m(x, t), therefore become

$$(1/V)\partial[Vc(x,t)]/\partial t = -k_g(x)c(x,t)\int_o^\infty m(x',t)dx' + \int_o^x k_g(x-x')c(x-x',t)m(x',t)dx' - k_d(x)c(x,t) + \int_x^\infty k_d(x')c(x',t)\delta(x-(x'-x_m))dx' - I\delta(x-x^*) \quad (3c)$$

and

$$(1/V)\partial[Vm(x,t)]/\partial t = -m(x,t)\int_o^\infty k_g(x')c(x',t)dx' + \int_x^\infty k_d(x')c(x',t)\delta(x-x_m)dx' + I\delta(x-x^*)x^*/x_m \quad (4b)$$

For a linear volume decrease due to solvent evaporation, $V(t)/V_0 = 1-\psi t$. A recently reported (Rabani et al., 2003) drying-mediated process for self-assembly of nanoparticles provides an opportunity to test the distribution kinetics approach. The work indicates that drying-mediated self-assembly of nanoparticles in 2-D occurs with a slope of 3/4 for average mass or volume versus time. Equivalently, the radius increases as a temporal power law with exponent 1/4. To simulate this process, we assume heterogeneous nucleation with evaporation of the solvent and solve Equations 3(c) and 4(b) for various values of Ψ (Figure 6(a)). With no evaporation of solvent ($\Psi = 0$), the asymptotic slope, b, is 6/7 for $\lambda = 1/3$ (solid line in Figure 6(a)). With increasing evaporation, the asymptotic slope gradually decreases, and a slope of 3/4 is obtained when Ψ is 10^{-4} with $\lambda = 1/3$ (dashed line in Figure 6(a)). This agreement with experimental results supports the proposed method of analysis. Various asymptotic slopes are obtained depending on the rate of evaporation, which indicates that drying-mediated self-assembly of nanoparticles in 2-D can be successfully simulated by the model.

To assess the effect of the power in rate coefficient expressions on the asymptotic slope, we choose $\lambda = 0$, 1/3, and 2/3, representing size-independent, diffusion-controlled, and surface-controlled processes. The power b approaches the long-time asymptotic value given by $(1-\lambda+1/d)^{-1}$, where d is the dimension. For $\lambda = 0$, the value of b is 2/3 and 3/4 for 2-D and 3-D, respectively. For 2-D, a slope of 3/4 is obtained when $\lambda = 1/6$. In addition to being consistent with the experimental results for drying-mediated self-assembly of nanoparticles, the model is consistent with the asymptotic slope obtained for size-independent, diffusion-controlled, and surface-controlled processes for both 2-D and 3-D systems, as predicted by the classical LSW theory.

Spinodal Decomposition

In contrast to the activated nucleation from a metastable solution, spinodal decomposition is a spontaneous, barrierless phase separation caused by forcing the system to become thermodynamically unstable. The classical spinodal is the curve denoting where the critical cluster (nucleus) vanishes. Within the metastable

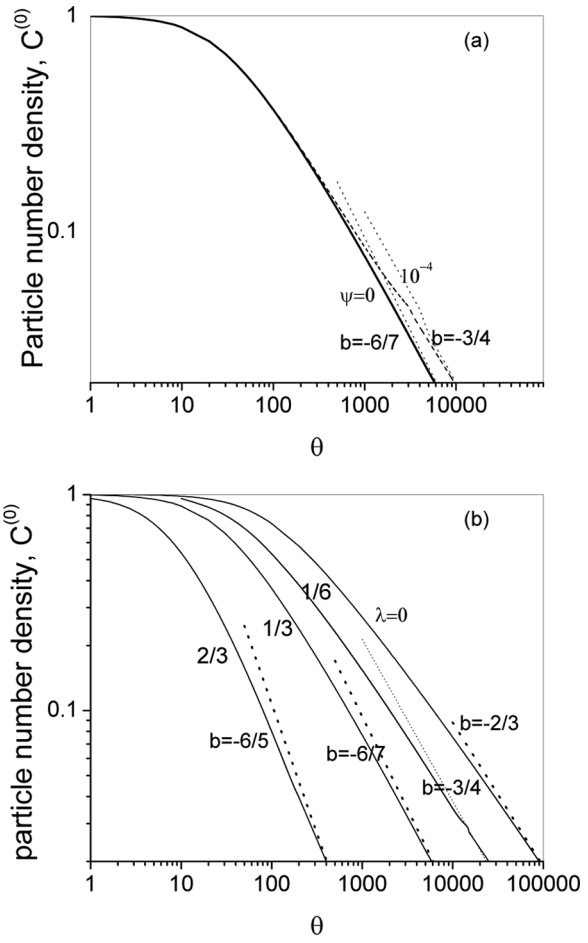

Figure 6. A self-assembly process driven by solvent evaporation. Effect of (a) evaporation and (b) exponent λ on the time evolution of the particle number density, $C^{(0)}(\theta)$, showing asymptotic power law decrease with time. The parameters used in the calculations are $\omega = 5$, $S_0 = 5$, with $C_0^{(0)} = 1$ and initial delta distribution centered at $C_0^{avg} = 75$. The dotted lines represent the asymptotic slopes, b.

region, nucleation gives rise to stable clusters that grow by rate-limited processes. For binary alloys, polymer mixtures, and vapor phase materials forced into the unstable spinodal region, a spontaneous phase separation occurs. When the nucleation barrier is vanishingly small (within the spinodal curve) unhindered cluster coalescence dominates the phase transition. Obviously, the kinetics and dynamics of interacting clusters provide the mechanism for such condensation phase transitions. For coalescence and breakage, the general model proposed by Smoluchowski (1916) allows clusters of all sizes to aggregate and for a cluster to split into unequal fragments. Monette and Klein (1992) recognized that coalescence of clusters is crucial for the occurrence of spinodal decomposition.

Spinodal decomposition has been traditionally studied by means of the Cahn-Hilliard theory (Cahn and Hilliard, 1958, 1959), which postulates that concentration fluctuations are governed by a diffusion mechanism. The cluster model provides a

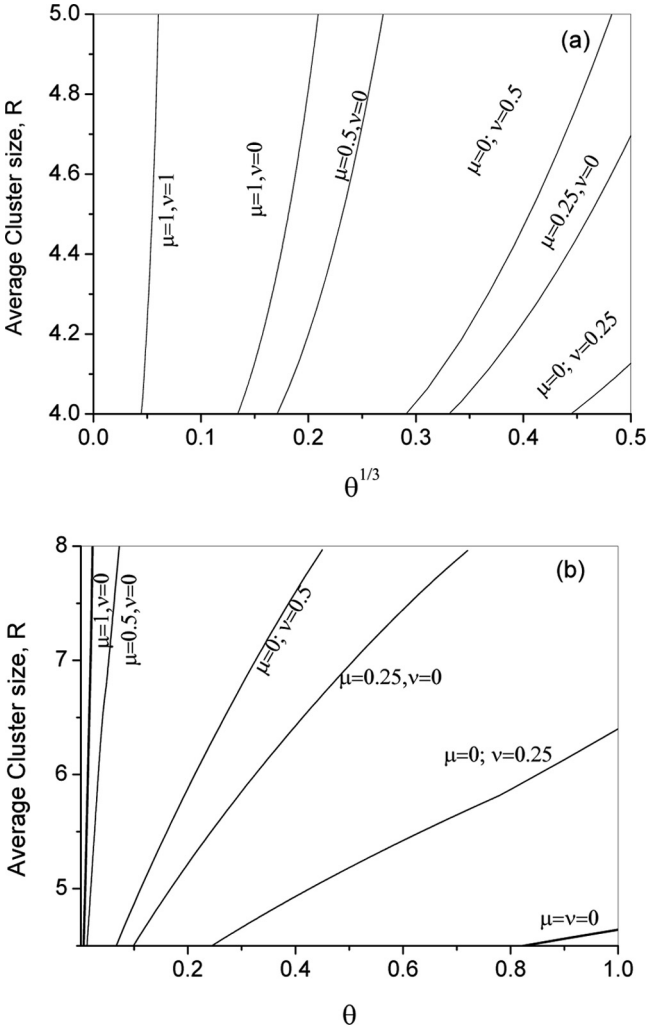

Figure 7. For spinodal decomposition, the time variation of the average cluster size, R, for (a) a plot versus $\theta^{1/3}$ to show power law relationship at early times and (b) a linear plot to show the linear variation at long times.

more clear-cut approach that transforms smoothly into models of nucleated transitions. Because the critical cluster size is less than one molecule, spinodal condensation is represented as a reversible aggregation-fragmentation cluster process. Experimental observations strongly demonstrate, however, that clusters rapidly combine into a single large phase, suggesting that the fragmentation process can be ignored. Formulating the aggregation rate coefficient as a general power expression, $k_a(x, x') = \kappa(xx')^{\mu}(x + x')^{\nu}$. For spherical dense phase domains, the average characteristic length is $R(\theta) = (3/4\,C^{avg}/N\pi\rho)^{1/3} = \alpha(C^{avg}(\theta))^{1/3}$, where ρ stands for the density of the dense phase domains and N is Avogadro's number. For simulation, α is assumed to be of the order of unity. Results (Yang et al., 2006b), shown in Figure 7, reveal how at early time the average cluster size increases with the 1/3 power of time, while the long time asymptote is nearly linear in time.

Gelation

Gelation is a fundamental phase transition process occurring in reacting polymers, hydrogels, and colloids and generally involves cluster aggregation and its reverse, fragmentation. Here the term cluster refers to aggregates of monomers that may be connected in branched or unbranched chains (each monomer has only one link to each of its nearest neighbors, except at branch points or chain ends) or in networks (monomers are interconnected by several links). By means of hydrolysis and condensation reactions, silica-based polycondensations with tetravalent Si yield a polymeric sol-gel. Reversible gelation (combined aggregation and fragmentation) is not only a general model for the phase transition dynamics, yielding the special cases of irreversible aggregation or fragmentation, but indeed is essential to describe mathematically the true microscopic kinetics and evolution to equilibrium or steady state. Modeling studies of reversible aggregation-fragmentation are based on population balance equations that govern the temporal evolution of continuous cluster-size distributions, c(x, t), in terms of the cluster mass x and time t.

Reversible gelation reactions occur in numerous polymer systems, for example, thermoreversible gels, hydrogels, polymer-clay solutions, and wheat gluten. Colloids undergo aggregation-fragmentation processes resembling reversible gelation and leading to solid-like elastic behavior (a jamming phase transition). When aggregation (or cross-linking) dominates over fragmentation (or chain scission), the mass or molecular weight of the clusters (macromolecules) increases, causing changes in rheological properties, including enhanced viscosity and the onset of viscoelasticity. Controlling the rheology of such responsive materials is an issue of controlling aggregation-fragmentation. Hydrogels dissolve when physical or chemical properties, e.g., temperature, ionic strength, or pH, are changed. Thermoreversible gels dissolve upon heating. Manipulating the character of a gel requires an understanding of the underlying kinetics and dynamics of cluster-size distributions during these processes.

Gelation is defined when the second and higher moments of the cluster-mass distribution diverge to infinity. Moment divergence causes properties of materials to change dramatically during gelation; for example, the viscosity sharply increases and elasticity is initiated. Moment divergence can occur before equilibrium is established for reversible aggregation-fragmentation systems.

We consider generally that clusters $\mathbf{C}(x)$ undergo aggregation and fragmentation as simultaneous binary processes. The breakage rate coefficient $k_b(x)$ will increase with size of the fragmenting cluster, $k_b(x) = \kappa_b x^{\nu_b}$, and the aggregation rate coefficient also has a power relationship in terms of the masses of two aggregating clusters, $k_a(x, x') = \kappa_a (xx')^{\nu_a} (x + x')^{\nu_o}$. The breakage rate coefficient prefactor κ_b , aggregation rate coefficient prefactor κ_a, and the powers ν_a, ν_b, and ν_o are constants. These parameters influence the mathematical solutions, including the gelation time. The values of the fragmentation coefficient, $\beta = k_{b0}/k_{a0}c_0^{(0)}$, and the exponent on fragmentation, ν_b, play important roles in determining whether gelation occurs. Figure 8 shows the variation of $(1 - \theta/\theta_c)$ with the mass-average molecular weight, $M_w = C^{(2)}/C^{(1)}$, on a log-log scale for various values of ν_a. Generally, the effects of aggregation parameters, ν_a and ν_o, are opposite those for fragmentation, ν_b and β.

Glassy Materials

When a fluid is cooled or compressed in a manner that avoids nucleation and crystallization, the resulting metastable (supercooled liquid) material is known as glass

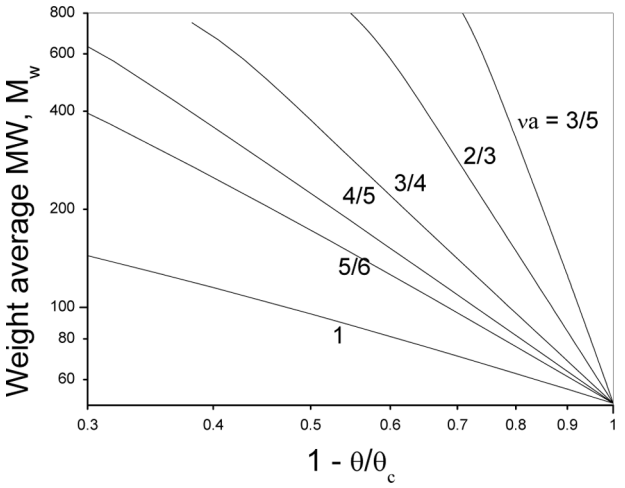

Figure 8. Variation of the weight-average molecular weight (M_w) with θ for various values of ν_a during gelation. Other kernel parameters are $\nu_o = 0$, $\beta = 0$, and the initial condition is a delta distribution with $C_0^{(0)} = 1$ and $C_0^{(1)} = 50$.

(Sastry, 2001; Debenedetti and Stillinger, 2001). The characteristic behavior is a huge, continuous increase in viscosity (or dielectric relaxation time) as the glassy material solidifies. Many modern materials, for example, in engineered plastics and optical and electronic materials, are glassy. Applying the clustering hypothesis (McCoy, 2002; Brenskelle and McCoy, 2006) has proved a reasonable way to derive correlations for viscosity as a function of temperature (or pressure) between the fluid and glass transition temperatures (or pressures). The fundamental mechanisms are aggregation and breakage, Equation (1), and monomer association and dissociation, Equation (2), to represent the fluctuating heterogeneous structures in the metastable liquid. The rate coefficients have temperature and pressure dependence given by transition state theory. Development of the zero moments, or molar concentrations, is sufficient to couple the free-volume theory to an expression for viscosity for the supercooled liquid. In accord with transition state theory for activated processes, the rate coefficients are proportional to $\exp(-E/k_BT - PV/k_BT)$, where E is the activation energy barrier and V is the activation volume. It ensues that viscosity has the expression $\eta = a\exp(b\Phi)$ where $\Phi = \exp[(h + Pv)/k_BT]$ in terms of $h = E_b - E_a - (E_d - E_g)$ and $v = v_b - v_a - (v_d - v_g)$. Clearly, any two conditions, for example $\eta_f = \eta(T_f, P)$ for the fluid and $\eta_g = \eta(T_g, P)$ for the glass transition temperatures, allow determination of the constants a and b. The resulting expression for $\eta = \eta(T, P)$ can be written as $\ln(\eta/\eta_g)/\ln(\eta_f/\eta_g) = (\Phi - \Phi_g)/(\Phi_f - \Phi_g)$ in terms of $\Phi_g = \exp[(h + Pv)/k_BT_g]$ and $\Phi_f = \exp[(h + Pv)/k_BT_f]$ and where η_f and η_g are of the order of 10^{-1} and 10^{14} poise, respectively. Plotting $\log \eta/\eta_g$ versus T_g/T (Figure 9) yields the fragility plot that is the basis for understanding dynamics of glassy materials.

Granular Systems

Granular materials—powders and granulated solids composed of particles in the size range from 10 μm to 3 mm in diameter—can exhibit both solid and fluid behavior.

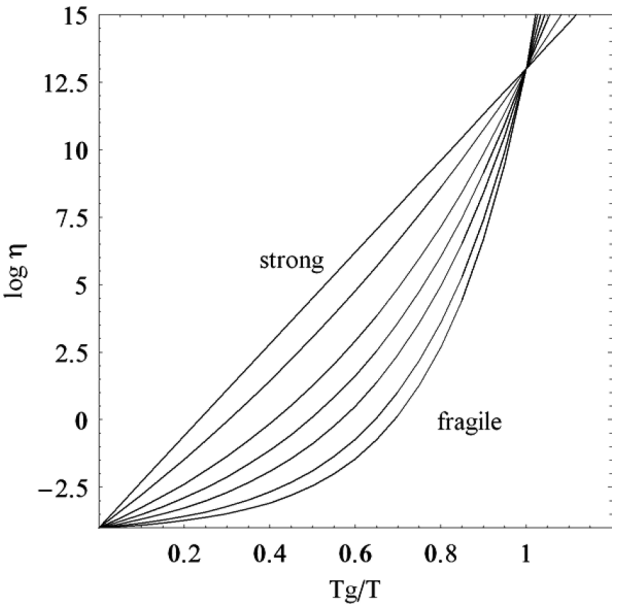

Figure 9. Fragility plot of the variation of glassy material viscosity with temperature as log η/η_g vs. T_g/T.

Owing to the very large number of particles involved, modeling of granular dynamics is based on statistical techniques. The models have numerous applications in industry as grains and particulate matter must be stored, moved, and mixed. In a new approach to granular materials, we have investigated the application of population balance (distribution kinetics) modeling to granular mixing (McCoy and Madras, 2005), compaction (McCoy and Madras, 2004), and separation (McCoy and Madras, 2006). The central concept in this treatment is the interaction of cluster-size distributions and single-particle (monomer) concentrations. Granular mixing (of powders, sand, seeds, grains, gravel, slurries) is often accomplished by tumbling operations, whereby loose particles slide down an inclined surface and/or particle clusters fragment and fall down the incline. In granular mixing equipment, splitting and recombining cause particles to move relative to one another and thus to mix. When interparticle attraction causes clustering, breaking up the clusters is essential to good mixing. When clustering does not occur because cohesion among particles is negligibly small, granular flows are often restricted to thin regions. Complications arise when the particles are not uniform, as subtle differences in physical properties can cause segregation, e.g., if particles differ in density and size. For analyzing mixing, we consider identical particles, with some marked as tracers. The interactions of individual particles and particle clusters can be described quantitatively by addressing the kinetics and dynamics of size-distributed clusters.

The physics of granular materials involves a range of conditions, but we focus on the typical state of particulates settled in a gravitational field and aggregated by interparticle forces. If the aggregate is tilted slightly, as in a tumbling operation, the individual particles on the surface may detach and slide, as in a surface flow (McCoy and Madras, 2006). If severely tilted, the aggregate itself may break apart,

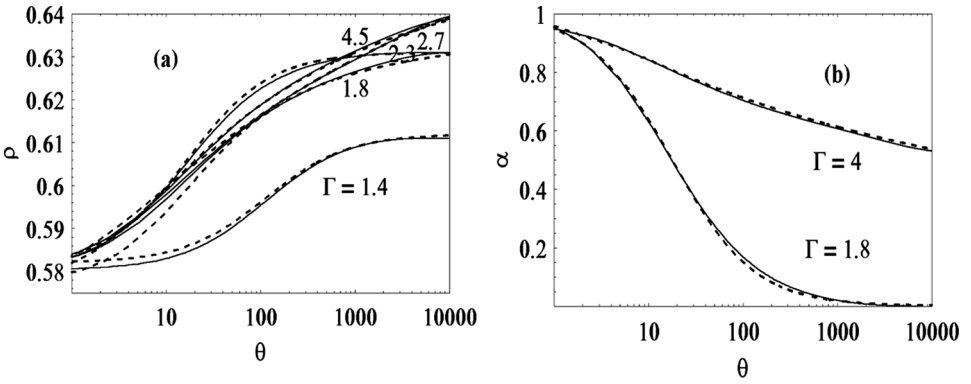

Figure 10. Comparison of granular density ρ versus time for the model (solid lines) with the experimentally based equations of (a) Knight et al. (1995) (dashed lines) and of (b) Linz (1996) (dashed lines).

with fragments cascading down as clusters or as an avalanche, thus allowing mixing. Analysis, design, and control of granular mixing have been difficult due to a lack of understanding of aggregation and breakup for these fundamental processes.

Of the many complex processes of granular materials, vibrational settling and compaction are common phenomena that have attracted much attention (McCoy and Madras, 2004). We have investigated vibrational, or tapping, compaction and propose that the underlying kinetics involves clusters fragmenting and aggregating and individual grains attaching and dissociating at cluster surfaces. The periodic vibrations cause cluster breakage and interchange between individual free grains and the clusters. We attribute this irreversibility to the growth of clusters, which, when formed, allow reversible changes for packing density ρ when Γ is either increased or decreased. The process is analogous to a phase transition with S playing the role of supersaturation and Γ representing energy input. The computations to compare with experimental data are quite easy and straightforward. The initial state consists almost entirely of free grains, and the clusters are assumed very small in the initial, loosely packed system. These tiny clusters act as seeds (heterogeneous nuclei) for cluster growth. The number of clusters, $c_0^{(0)}$, decreases with aggregation to the final steady-state value, $c_s^{(0)}$. The experimental data of Knight et al. (1995) and Linz (1996) are well simulated by the theory (Figure 10).

Segregation of large particles in a granular medium can be investigated with the cluster kinetics approach (McCoy and Madras, 2006). The Brazil-nut effect is an example: larger particles rise to the top of a granular medium composed of smaller grains. The granules form clusters that fragment and aggregate, providing a heterogeneous medium in which an immersed particle rises due to the interaction of viscous drag and buoyancy forces. The model explains experimental data showing a maximum in rise time (or rise velocity) in terms of particle radius, initial depth of the particle, and particle/grain density ratio.

Oscillator Synchronization

Collective synchronization of oscillators occurs in many natural and engineered systems and has attracted much research attention to understand its behavior.

Populations of coupled limit-cycle oscillators tend to synchronize by altering their frequencies and phase angles. Observations of coupled oscillators (Winfree, 1967), such as groups of chorusing crickets (Walker, 1969), flashing fireflies (Buck, 1988), and cardiac pacemaker cells (Peskin, 1975), reveal a spontaneous transition from incoherence to collective synchronization beyond a threshold in coupling strength (Kuramoto, 1975). The process is similar to a condensation phase transition, e.g., crystallization, with monomers attaching to clusters. The grouping, or clustering, can occur only when the coupling is of sufficient strength to grow the synchronized-oscillator cluster. If the coupling is too weak, the oscillators will not synchronize. This is similar to crystallization for which the phase transition can occur only if the liquid is supersaturated, that is, in a metastable state. An undersaturated system of crystals will dissolve, just as oscillators may desynchronize. The hypothesis is that oscillator synchronization is the reversible addition of individual oscillators to a synchronized cluster. The oscillators begin in an incoherent state and freeze into coherence by synchronization. Synchronization of the oscillator phase angle is governed by nonlinear dynamics that can be mathematically described by the "phase models" (e.g., by Daido (1990, 1994, 1996) and Kuramoto (1984a,b)) as mentioned by Strogatz (2000).

Synchronization is here considered the growth of a coherent cluster by the addition of individual oscillators M onto the cluster $\mathbf{C}(x)$ composed of x synchronized oscillators:

$$\mathbf{C}(x) + \mathbf{M} \underset{k_d(x)}{\overset{k_g(x)}{\rightleftarrows}} \mathbf{C}(x+1) \tag{15}$$

This reversible process allows for oscillators to synchronize or to desynchronize. The corresponding rate coefficients are $k_g(x)$ and $k_d(x)$ for growth and dissociation, respectively. We assume, in parallel with crystallization, that the growth and dissociation rates increase as a power of size, $k_g(x) = \kappa_g x^{\lambda}$ and $k_d(x) = \kappa_d x^{\lambda}$. For $\lambda > 0$, larger clusters recruit more incoherent oscillators into the synchronized cluster. Oscillators proceed through exponential time dependence before taking on power law behavior at intermediate times, as reported for model computations (Madras and McCoy, 2008). The power varies for synchronization and depends on the rate coefficient but is constant for desynchronization. In terms of the coupling constant K and its critical value K_c, the coherence increases as $(1 - K_c/K)^{\beta}$, where $\beta = 1$, the generic value (Daido, 1990, 1994, 1996), rather than $1/2$, the special case for sinusoidal coupling (Kuramoto, 1975). The long-time limit is a stationary equilibrium state. The bifurcation plots of long-time coherence and coupling rate coefficient are shown in Figure 11.

Future Applications

Among the new methods of crystallization, anti-solvent (also known as extractive or salting-out) crystallization is an interesting energy-saving alternative to evaporative crystallization, provided that the anti-solvent can be separated easily at lower energy costs. In this method, the anti-solvent decreases the solvent power of the primary solvent and causes the precipitation of the solid. The key idea behind the technique is to use anti-solvents whose miscibility with the saturated solvent is a strong function of

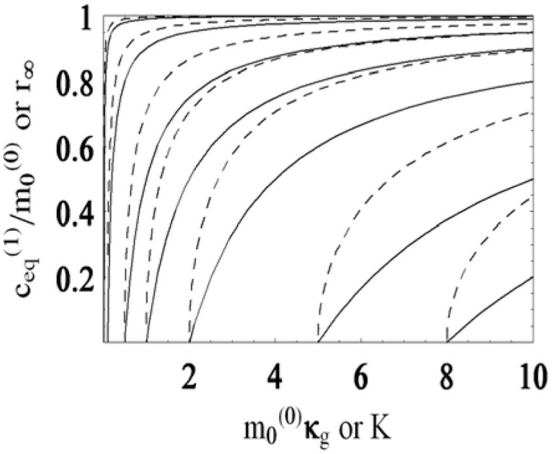

Figure 11. Fundamental behavior of oscillator synchronization. Bifurcation plots of long-time coherence versus coupling rate coefficient for $K_c = \kappa_d = 0.01$, 0.1, 0.5, 1.0, 2.0, 5.0, 8.0 (left to right, where the curves intersect the horizontal axis); solid line is the prediction of Daido (1994, 1996) and of the present model, dashed line is the Kuramoto (1984a,b) model.

temperature. Acetone was used as an anti-solvent to precipitate potassium sulfate from an aqueous solution (Jones et al., 1987) with the finding that small dilutions due to the anti-solvent improved the permeability of the crystal cake by reducing excessive nucleation. Anti-solvent crystallization has also been used to control particle size distribution during the crystallization of sodium chloride (Doki et al., 2002) and for the crystallization of paracetamol (Granberg et al., 1999; Fujiwara et al., 2002). The effect of agitation, feeding rate, and the evolution of the particle mean size has been reported for the anti-solvent crystallization of paracetamol with a water-acetone mixture (Yu et al., 2005). The continuous distribution model can be applied to anti-solvent crystallization by including in Equations (3c) and (4b) the rate of anti-solvent addition in V(t).

Because of environmental restrictions on common volatile solvents, supercritical fluids are widely used in micronization technologies. Among them, the *gas* or *supercritical anti-solvent* (GAS or SAS) process is popular because several kinds of materials, including explosives, polymers, pigments, and pharmaceuticals, can be micronized with this technique (Martin and Cocero, 2004). Many studies on this process have investigated only the effect of various operating variables on the morphology and size distribution of particles formed. However, for the design of new experiments, a robust theoretical model should be based on the phase equilibrium, mass transfer, fluid mechanics of the mixing between the organic solution and the supercritical anti-solvent, and kinetics of particle nucleation and growth. We propose that clustering and declustering are at the core of this process and that the population balance approach discussed in this work is suited for its modeling.

Another potential application is metal-organic vapor-phase epitaxy. For example, zinc oxide is widely used in surface acoustic wave (SAW) devices, transparent conductive films, and light emitting diodes (LEDs). The substrate for zinc oxide growth is usually an insulator-like sapphire and cannot be applied for making vertical geometry devices like conventional GaAs LEDs. The growth of these

materials on conductive material substrates has been hindered (Moriyama and Fujita, 2007) due to easy oxidation and lack of control of growth of the nucleation layer and the main layer. Because the theory discussed in this work covers the complete transition from nucleation to growth to Ostwald ripening, the model seems applicable to metal-organic vapor-phase epitaxy.

Chemical vapor deposition (CVD) processes are widespread for manufacturing microelectronic components, automotive parts, optical devices, magnetic materials, and semiconductors. In the semiconductor industry, CVD is used to deposit a variety of films, such as polysilicon and epitaxial silicon. Controlling the purity of the film is of paramount importance in silicon epitaxy processes. The presence of impurities in the semiconductor material can lead to an excess of holes or free electrons, resulting in poor properties, and is one of the major limitations for the efficient processing of semiconductors (Kommu et al., 2004). Particulate impurities can be generated inside a CVD reactor through chemical processes such as the gas phase reactions between $SiHCl_3$ and H_2 used for growing epitaxial films (Kommu et al., 2000). Mathematical models that account for the basic mechanisms for particle generation and transport within CVD reactors need to be developed. While models that account for flow patterns and heat and mass transfer and models (Kleijn and Hoogendoorn, 1991) that include multiple chemical reactions (Ho et al., 1998) have been developed to predict epitaxial deposition rates, models that describe the particle dynamics within CVD reactors are lacking. The particle dynamics can be numerically simulated by the Lagrangian approach for large-sized particles and the Eulerian approach for small-sized particles. The Lagrangian model (Davis et al., 1993) for CVD reactors has been successfully used for particle sizes greater than 1 μm. However, because the impurities are usually due to smaller particles, models based on the Eulerian approach are needed. A comprehensive model based on this approach incorporating the key mechanisms of particle transport, nucleation, condensation, and aggregation has been developed (Friedlander, 2000). A detailed clustering mechanism for particle formation based on a log-normal particle size distribution coupled with a kinetic model has been developed (Girshick et al., 2000). Though detailed nucleation rate expressions are normally not available for reactions occurring in CVD systems, the classical theory based on the concept of thermodynamic pseudo-equilibrium can predict nucleation rates (Seinfeld and Pandis, 1997) at low temperatures or atomistic models can be used for the nucleation rates (Zachariah and Tsang, 1995). Unlike the model we have proposed, many nucleation and growth models ignore that particles below the smallest thermodynamically stable particle sizes are unstable and transitory. For example, it has been arbitrarily assumed (Girshick et al., 2000) that compounds containing 10 silicon atoms are the smallest sized particles. For species having low equilibrium vapor pressure, however, it has been shown that even single molecules are thermodynamically stable and the thermodynamic critical particle diameter can be set equal to the diameter of a monomer molecule (Ulrich, 1971). An accurate kinetic model for $SiHCl_3$ decomposition needs to be coupled with the above-described transport model for silicon epitaxy. There is considerable information available regarding intrinsic kinetic and thermochemical processes associated with gas phase (Swihart and Carr, 1998), surface chemistry (Walker et al., 1998), and reaction mechanism (Ho et al., 1985) of $SiHCl_3$. The comprehensive model described in this work includes nucleation, crystal growth, condensation, and aggregation and can be coupled with intrinsic kinetic models available in the literature and can thus potentially be applied to model CVD processes.

Synthesis of structural nanocrystalline ceramics that would possess desirable properties like hardness, strength, and abrasion resistance is a challenge because of the difficulties in fabricating large three-dimensional parts from nanocrystalline powders. Compaction of powders is usually done at high temperatures and pressures. However, these techniques can cause grain growth and coarsening, such that the desirable properties observed at the nanometer grain size are not achieved at a large scale. Alternative methods (Suryanarayana, 2002; Chraska et al., 2008) to produce bulk nanocrystalline materials by avoiding the powder compaction step have been developed by initially producing an amorphous material followed by rapid solidification and controlled crystallization. Such materials are usually fully nanocrystalline or in the form of a nanocomposite in which the nanometric crystallites are dispersed in the original amorphous phase. The theoretical model described here includes variables for temperature-controlled crystallization and thus can be applied to this process. For example, the temperature in Equations (3a), (3b), and (4a) can be written explicitly as a function of time (Madras and McCoy, 2004), and the kinetics of nucleation, growth, and denucleation can be determined as a function of both temperature and time.

Subsequent to the discovery of the high permittivity of ferroelectric materials, ceramic materials based on these compounds have been utilized for manufacturing electronic devices such as transducers, thermal switches, capacitors, and memory storage devices. Glass-ceramics are polycrystalline materials produced by crystallization of glasses using specific heat treatment procedures. Due to superior thermal, mechanical, and electrical properties compared to their parent glasses, glass-ceramics have numerous applications in the electronics, cookware, and biomedical industries. Despite this, there has been a lack of the study of the fundamental properties of glass-ceramics (Kim et al., 2007), which are dependent on the crystal volume fraction and crystal size in the glass matrix.

In the process of conversion of glass to glass-ceramics, controlled crystallization plays an important role in engineering the different physicochemical properties (Goswami et al., 2007). The production of glass-ceramics involves two primary steps: the preparation of a homogeneous glass followed by the application of a controlled heat treatment process. The latter step consists of nucleation wherein the glass is maintained at the nucleation temperature until stable nuclei are formed, followed by an increase in temperature wherein crystal growth occurs (Erol et al., 2007). Understanding the fundamental processes of nucleation and crystallization in glasses is of paramount importance in preparing glass-ceramics with desired microstructures and properties (Xu et al., 1991).

Cordierite glass-ceramics belong to a special class of glass-ceramics because of their superior electrical insulation, ultrahigh vacuum compatibility, low thermal conductivity, high thermal stability, and excellent mechanical strength (Baik et al., 1995; Pannhorst, 1997; Xu and Jahanmir, 1999) and find applications in areas where high-temperature creep resistance and high resistance to thermal shock are required (McMillan, 1979). Although a number of studies have examined the relationship between phase separation, nucleation, and crystallization in the cordierite glasses (Muller, 1989; Amista et al., 1995) and in determining the kinetic parameters (Barry et al., 1970; Tomozama, 1971), more comprehensive data are required before a clearer understanding of the crystallization processes can emerge (Goel et al., 2007). Because the continuous distribution kinetic approach discussed in this work accounts for the crystal volume fraction and crystal size and treats the transition

from nucleation and crystal growth naturally as a function of time and temperature, it can be used to describe crystallization in glass-ceramics.

Microscale inorganic materials with well-defined morphology have attracted considerable attention for their structural characteristics endowing them with a wide range of potential applications. However, fabrication of inorganic materials with controllable morphology is still a great challenge in material science. Synthesis of well-crystallized microspheres assembled with nanoparticles requires knowledge of nucleation, growth, self-assembly, and evaporation in solvothermal reduction. The proposed model, by accounting for all these variables, provides a viable method.

Active pharmaceutical ingredients (APIs) are frequently delivered to the patient as tablets or capsules. Storing these APIs as solids is convenient and compact. Understanding and controlling the solid-state chemistry of APIs is an important aspect of the drug development process. APIs can exist as polymorphs, solvates, hydrates, salts, co-crystals, and amorphous solids. Each form displays unique physicochemical properties that influence the bioavailability, stability, and other performance characteristics of the drug (Bryn et al., 1999). Therefore, it is vital to investigate and understand the relationship between the particular solid form of a compound and its functional properties. Importantly, the desired properties may vary with the type of delivery (i.e., oral, pulmonary, transdermal, etc.), such that the solid form may differ for each optimized dosage form. Given these options, the choice and design of pharmaceutical solid forms can be critically important to successful drug development. The cluster models described in this review provide a framework for understanding the phenomena associated with pharmaceutical manufacture and use.

Many drug delivery systems are polymeric where the polymer network forms a matrix for encapsulation, and the subsequent delivery of the drug is controlled. Several processes like diffusion, hydration, gelation, and swelling govern the rate of release of a drug from a hydrophilic matrix following addition to a dissolution medium. Clearly knowledge of, and control over, these characteristics is essential to tailor drug release to a specific pharmacological profile (Maggi et al., 2002). The cluster distribution models described here can include these phenomena and model the drug delivery systems.

Hydrogels are water-swollen polymer networks that are receiving interest as biomedical materials (Hoffman, 2002), superabsorbent materials (Kabiri et al., 2003), and sensors (Davies and Tighe, 1991). Model hydrogels with well-defined molecular architecture can be synthesized by end-linking reactions. The polymer concentration at cross-linking strongly affects gelation and swelling behavior, as diluting the reaction mixture with water increases the average separation between dendrimers, forming many intramolecular loops at the expense of elastically effective network chains. Our model of gelation includes the effect of polymer concentration and also shows how the molecular weight distribution evolves as gelation is approached.

Several commercial polymers like poly(ethylene terephthalate) (PET) have molecular chains connected with aromatic, ethyl, and ester groups. The twist or torque motion between rigid aromatic segments and the alkyl connector significantly reduces the rate of crystallization and slows the processing cycle. The maintenance of a balance between enhancing PET crystallization rate and retaining its original overall properties is a key problem that relies on the control of the nucleation and growth process of crystallization (Imai and Kaji, 2006; Bassett, 2006). Nanocomposites afford good dispersion of nanoparticles by controlled nucleation and growth of

crystals in the polymer. Their nucleation and crystallization behaviors under isothermal and non-isothermal conditions have been quantitatively investigated (Ke et al., 2007), but the conventional theories do not apply. The theory described in this work can potentially be applied for the crystallization of these nanocomposites, possibly providing a clear fundamental understanding of the underlying mechanisms. Polyolefins like poly(4-methyl-1-pentene) (iP4MP1) are widely used as membranes. Several crystalline polymorphs exist for these polymers depending on the solvent and thermal history of the crystallization. Recently, attempts have been made to study the crystallization and gelation behavior of these polymers in supercritical fluids (Fang and Kiran, 2006) that can yield new forms. Modeling the crystallization and gelation in supercritical fluids is a challenge for the fundamental approach proposed in our model.

Biomaterials such as shells and bones consist of inorganic single crystals intergrown with organic material with the crystals showing a remarkable degree of preferential alignment. To develop these materials synthetically, thin films are deposited on substrates under ultrahigh vacuum. The structure and morphology of the deposited film depend on several parameters including nucleation and structure of the substrate surface. Several studies have investigated nucleation under Langmuir monolayers (Kewalramani et al., 2007), growth as specific polymorphs, and operating conditions such as temperature, monolayer pressure, and pH. A complete theory that accounts for all the stages of nucleation, separation of polymorphs, and development of monolayers, as described in the current study, may be applicable in synthesizing new biomaterials.

In modeling microbial cultures, experimental results and mathematical models representative of average cell behavior are scaled to the cell population, though individual cells exhibit heterogeneity as a result of differences in their cellular metabolism and cell-cycle dynamics. To develop a fundamental understanding of cell heterogeneities and their effects on microbial population dynamics, population balance equation models, in which the intracellular state is characterized by additional variables, may be useful. Such models, with either discrete or continuous variables, could be valuable for dynamic simulation and analysis and for the development of on-line fermenter monitoring and control schemes (Henson, 2003; Mantzaris et al., 1999).

Conclusions

Phase transition dynamics constitute a central aspect of many of the new methods of chemical fabrication and manufacture. The chemical industries have been keystones of the energy, transportation, industrial chemical, agriculture, and food processing industries for centuries. Now chemical engineering is making innovative progress in pharmaceutical, materials, electronics, biotechnology, and environmental areas. Many of the innovations are more complex, smaller in scale, and more sensitive to ambient conditions than conventional processes. They require a deeper knowledge and understanding of the dynamics of the underlying physical and chemical phenomena. As we have attempted to explain, phase transitions are important in a large number of these new processes and techniques.

By definition, phase condensation involves collecting molecular units into more dense aggregates, or clusters; hence, we have focused on cluster kinetics and dynamics in this review. The concepts of clustering are frequently used in narratives

describing phase transitions, but quantitative, mathematical representations have been rare until recently. As expected of a molecular process such as phase condensation, dynamic behavior is always prevalent, even when the system reaches (dynamic) equilibrium. We have proposed that the fundamental cluster processes are represented by the reversible aggregation mechanisms of Equations (1) and (2). Through the mathematics of population balance modeling, one can characterize the kinetics of cluster aggregation and fragmentation and monomer addition and dissociation. Like other subjects in chemical engineering science, e.g., transport phenomena and chemical kinetics, distribution kinetics affords vital functional and scaling characteristics. Knowledge of exponential or power dependence of properties (moments) on time, for instance, is crucial to understanding observed behavior. More detailed quantitative information must, at present, rely on experimental measurements. This is similar to transport phenomena and chemical kinetics, for which transport parameters and rate constants are generally measured experimentally. Only in certain special cases can these parameters be related to more fundamental molecular theories, for example, transport coefficients calculated from kinetic theory of gases or rate constants from quantum mechanics.

References

Amista, P., Cesari, M., Montenero, A., Gnappi, G., and Lan, L. (1995). Crystallization behaviour in the system MgO—Al_2O_3—SiO_2, *J. Non-Cryst. Solids*, **529**, 192–193.

Avrami, M. (1939). Kinetics of phase change. I: General theory, *J. Chem. Phys.*, **7**, 1103.

Avrami, M. (1940). Kinetics of phase change. II transformation-time relations for random distribution of nuclei, *J. Chem. Phys.*, **8**, 212.

Ayazi Smalou, P., Jones, A. G., and Djamarani, K. (1990). Hydrodynamics of secondary nucleation in suspension crystallization, *Chem. Eng. Sci.*, **45**, 1405.

Baik, D. S., No, K. S., and Chun, J. S. (1995). Mechanical properties of mica glass–ceramics, *J. Am. Ceram. Soc.*, **78**, 1217.

Barry, T. I., Clinton, D., Lay, L. A., Mercer, R. A., and Miller, R. P. (1970). The crystallisation of glasses based on the eutectic compositions in the system Li2O-Al2O3-SiO2 - Part 2 Lithium metasilicate-B-eucryptite, *J. Mater. Sci.*, **5**, 117.

Bassett, D. C. (2006). Linear nucleation of polymers, *Polymer*, **47**, 5221.

Becker, R. and Doring, W. (1935). The kinetic treatment of nuclear formation in supersaturated vapors, *Ann. Phys. NY*, **24**, 719.

Bhakta, A. and Ruckenstein, E. (1995). Ostwald ripening: A stochastic approach, *J. Chem. Phys.*, **103**, 7120.

Bolton, C. D. and Wattis, J. A. D. (2002). General Becker-Doŕing equations: Effect of dimer interactions, *J. Phys. A Math. Gen.*, **35**, 3183.

Brenskelle, L. A. and McCoy, B. J. (2006). Cluster kinetics of pressure-induced glass formation, *J. Chem. Phys.*, **124**, 084502.

Buck, J. (1988). Synchronous rhythmic flashing of fireflies. II, *Q. Rev. Biol.*, **63**, 265.

Byrn, S. R., Pfeiffer, R. R., and Stowell, J. G. (1999), *Solid-State Chemistry of Drugs*, SSCI, West Lafayette, Ind.

Cahn, J. W. and Hilliard, J. E. (1958). Free energy of a nonuniform system. I. interfacial free energy, *J. Chem. Phys.*, **28**, 258.

Cahn, J. W. and Hilliard, J. E. (1959). Free energy of a nonuniform system. III. Nucleation in a two-component incompressible fluid, *J. Chem. Phys.*, **31**, 688.

Chraska, T., Neufuss, K., Dubsky, J., Ctibor, P., and Rohan, P. (2008). Fabrication of bulk nanocrystalline alumina-zirconia materials, *Ceram. Int.*, **34**(5), 1229–1236.

Daido, H. (1990). Intrinsic fluctuations and a phase transition in a class of large populations of interacting oscillators, *J. Stat. Phys.*, **60**, 753.

Daido, H. (1994). Generic scaling at the onset of macroscopic mutual entrainment in limit-cycle oscillators with uniform all-to-all coupling, *Phys. Rev. Lett.*, **73**, 760.

Daido, H. (1996). Onset of cooperative entrainment in limit-cycle oscillators with uniform all-to-all interactions: Bifurcation of the order function, *Physica D*, **91**, 24.

Davies, M. L. and Tighe, B. J. (1991). Potential of hydrogen polymers in sensor applications, *Sel. Electrode Rev.*, **13**, 159.

Davis, R. W., Moore, E. F., and Zachariah, M. R. (1993). Numerical modeling of particle dynamics in a rotating disk chemical vapor deposition reactor, *J. Cryst. Growth*, **132**, 513.

Debenedetti, P. G. (1996). *Metastable Liquids: Concepts and Principles*, Princeton University Press, Princeton, N.J.

Debenedetti, P. G. and Stillinger, F. G. (2001). Supercooled liquids and the glass transition, *Nature(London)*, **410**, 259.

Doki, N., Kubota, N., Yokota, M., Kimura, S., and Sasaki, S. (2002). Production of sodium chloride crystals of uni-modal size distribution by batch dilution crystallization, *J. Chem. Eng. Jpn.*, **35**, 1099.

Erol, M., Kucukbayrak, S., and Ersoy-Mericboyu, A. (2007). Production of glass-ceramics obtained from industrial wastes by means of controlled nucleation and crystallization, *Chem. Eng. J.*, **132**, 335.

Evans, U. R. (1945). The laws of expanding circles and spheres in relation to the lateral growth of surface films and the grain-size of metals, *Trans. Faraday Soc.*, **41**, 365.

Fang, J. and Kiran, E. (2006). Crystallization and gelation of isotactic poly(4-methyl-1-pentene) in n-pentane and in n-pentane + CO2 at high pressures, *J. Supercrit. Fluids*, **38**, 132.

Friedlander, S. K. (2000). *Smoke, Dust and Haze: Fundamentals of Aerosol Dynamics*, 2nd, ed., Oxford University Press, New York.

Fujiwara, M., Chow, P. S., Ma, D. L., and Braatz, R. D. (2002). Paracetamol crystallization using laser backscattering and ATR-FTIR spectroscopy: Metastability, agglomeration, and control, *Cryst. Growth Des.*, **2**, 363.

Girshick, S. L., Swihart, M. T., Suh, S. M., Mahajan, M. R., and Nijhawan, S. (2000). Numerical modeling of gas-phase nucleation and particle growth during chemical vapor deposition of silicon, *J. Electrochem. Soc.*, **147**, 2303.

Goel, A., Shaaban, E. R., Melo, F. C. L., Ribeiro, M. J., and Ferreira, J. M. F. (2007). Non-isothermal crystallization kinetic studies on MgO-Al2O3-SiO2-TiO2 glass, *J. Non-Cryst. Solids*, **353**, 2383.

Goswami, M., Sengupta, P., Sharma, K., Kumar, R., Shrikhande, V. K., Ferreira, J. M. F., and Kothiyal, G. P. (2007). Crystallization behaviour of Li_2O{single bond}ZnO{single bond}SiO2 glass-ceramics system, *Ceram. Int.*, **33**, 863.

Granberg, R. A., Bloch, D. G., and Rasmuson, A. C. (1999). Crystallization of paracetamol in acetone-water mixtures, *J. Cryst. Growth*, **199**, 1287.

Groot, S. R. de and Mazur, P. (1962). *Non-Equilibrium Thermodynamics*, North-Holland, Amsterdam.

Hay, J. N. (1971). Application of the modified avrami equations to polymer crystallisation kinetics, *Br. Polym. J.*, **3**, 74.

Henson, M. A. (2003). Dynamic modeling of microbial cell populations, *Curr. Opin. Biotechnol.*, **14**, 460.

Ho, P., Coltrin, M. E., Binkley, J. S., and Melius, C. F. (1985). A theoretical study of the heats of formation of SiHn, SiCln, and SiHnClm compounds, *J. Phys. Chem.*, **89**, 4647.

Ho, P., Balakrishna, A., Chacin, M. J., and Thilderkvist, A. (1998). Chemical kinetics for modeling Silicon epitaxy from chlorosilanes. In: *Proceedings of the Symposium on Fundamental Gas-Phase and Surface Chemistry of Vapor-Phase Materials Synthesis*, eds. M. D. Allendorf et al., Electrochemical Society, Pennington, N.J.

Hoffman, A. S. (2002). Hydrogels for biomédical applications, *Adv. Drug Deliv. Rev.*, **54**, 3.

Imai, M. Y. and Kaji, K. S. (2006). Polymer crystallization from the metastable melt: The formation mechanism of spherulites, *Polymer*, **47**, 5544.

Jones, A. G., Budz, J., and Mullin, J. W. (1987). Crystallization and solid-liquid separation of potassium sulphate crystals, *Chem. Eng. Sci.*, **42**, 619.

Kabiri, K., Omidian, H., Hashemi, S. A., and Zohuriaan-Mehr, M. J. (2003). Synthesis of fast-swelling superabsorbent hydrogels: Effect of crosslinker type and concentration on porosity and absorption rate, *Eur. Polym. J.*, **39**, 1341.

Ke, Y.-C., Wu, T.-B., and Xia, Y.-F. (2007). The nucleation, crystallization and dispersion behavior of PET-monodisperse SiO_2 composites, *Polymer*, **48**(11), 3324–3336.

Kewalramani, S., Kmetko, J., Dommett, G., Kim, K., Evmenenko, G., Mo, H., and Dutta, P. (2007). Pathways for oriented assembly of inorganic crystals at organic surfaces, *Thin Solid Films*, **515**, 5627.

Kim, J. E., Song, C. H., Park, H. W., Ohshima, K.-I., and Yang, Y. S. (2007). Kinetics of crystallization in $4BaTiO_3$-SiO_2 glass, *Mater. Sci. Eng. A*, **449–451**, 299–301.

Kleijn, C. and Hoogendoorn, C. J. (1991). A study of 2- and 3-D transport phenomena in horizontal chemical vapor deposition reactors, *Chem. Eng. Sci.*, **46**, 321.

Knight, J. B., Fandrich, C. G., Lau, C. N., Jaeger, H. M., and Nagel, S. R. (1995). Density relaxation in a vibrated granular material, *Phys. Rev. E*, **51**, 3957.

Kommu, S., Wilson, G. M., and Khomami, B. (2000). Theoretical/experimental study of silicon epitaxy in horizontal single-wafer chemical vapor deposition reactors, *J. Electrochem. Soc.*, **147**, 1538.

Kommu, S., Khomami, B., and Biswas, P. (2004). Simulation of aerosol dynamics and transport in chemically reacting particulate matter laden flows. Part II: Application to CVD reactors, *Chem. Eng. Sci.*, **59**, 359.

Kuramoto, Y. (1975). Coherence in a population of chemical oscillators. In: *International Symposium on Mathematical Problems in Theoretical Physics*, Springer-Verlag, Berlin.

Kuramoto, Y. (1984a). *Chemical Oscillations, Waves, and Turbulence*, Springer-Verlag, Berlin.

Kuramoto, Y. (1984b). Cooperative dynamics of oscillator community – a study based on lattice of rings, *Prog. Theor. Phys. Suppl.*, **79**, 223.

Laurençot, P. and Mischler, S. (2002). From the Becker-Döring to the Lifshitz-Slyozov-Wagner equations, *J. Stat. Phys.*, **106**, 957.

Lifshitz, I. M. and Slyozhov, J. (1961). The kinetics of precipitation from supersaturated solid solutions, *J. Phys. Chem. Solids*, **19**, 35.

Linz, S. J. (1996). Phenomenological modeling of the compaction dynamics of shaken granular systems, *Phys. Rev. E*, **54**, 2925.

McCoy, B. J. (2002). Cluster kinetics for glassforming materials, *J. Chem. Phys. Solids*, **63**, 1967.

McCoy, B. J. and Madras, G. (1997). Degradation kinetics of polymers in solution: Dynamics of molecular weight distributions, *AIChE J.*, **43**, 802.

McCoy, B. J. and Madras, G. (2004). Cluster kinetics of density relaxation in granular materials, *Phys Rev. E*, **70**, 051311.

McCoy, B. J. and Madras, G. (2005). Cluster kinetics of granular mixing, *AIChE J.*, **51**, 406.

McCoy, B. J. and Madras, G. (2006). Cluster kinetics model of particle separation in vibrated granular media, *Phys. Rev. E*, **73**, 011301.

McMillan, P. W. (1979). *Glass-Ceramics*, 2nd ed., Academic, London.

Madras, G. and McCoy, B. J. (1998). Time evolution to similarity solutions for polymer degradation, *AIChE J.*, **44**, 647.

Madras, G. and McCoy, B. J. (2001). Molecular-weight distribution kinetics for ultrasonic reactions of polymers, *AIChE J.*, **47**, 2341.

Madras, G. and McCoy, B. J. (2002). Dynamics of crystal size distributions with size-dependent rates, *J. Cryst. Growth*, **243**, 204.

Madras, G. and McCoy, B. J. (2003). Growth and ripening kinetics of crystalline polymorphs, *Cryst. Growth Des.*, **3**, 981.

Madras, G. and McCoy, B. J. (2004). Temperature effects on the transition from nucleation and growth to Ostwald ripening, *Chem. Eng. Sci.*, **59**, 2753.
Madras, G. and McCoy, B. J. (2006). A distribution kinetics model of self-assembly: Effects of coalescence and solvent evaporation, *J. Crys. Growth*, **286**, 131.
Madras, G. and McCoy, B. J. (2008). Cluster kinetics and dynamics of oscillator synchronization, *Int. J. Mod. Phys.*, **22**(7), 889–900.
Maggi, L., Segale, L., Torre, M. L., Ochoa Machiste, E., and Conte, U. (2002). Dissolution behaviour of hydrophilic matrix tablets containing two different polyethylene oxides (PEOs) for the controlled release of a water-soluble drug. Dimensionality study, *Biomaterials*, **23**, 1113.
Mantzaris, N. V., Liou, J.-J., Daoutidis, P., and Srienc, F. (1999). Numerical solution of a mass structured cell population balance model in an environment of changing substrate concentration, *J. Biotechnol.*, **71**, 157.
Marqusee, J. A. and Ross, J. (1983). Kinetics of phase transitions: Theory of Ostwald ripening, *J. Chem. Phys.*, **79**, 373.
Martín, A. and Cocero, M. J. (2004). Numerical modeling of jet hydrodynamics, mass transfer, and crystallization kinetics in the supercritical antisolvent (SAS) process, *J. Supercrit. Fluids*, **32**, 203.
Mazzarotta, S., Di Cave, S., and Bonifazi, G. (1993). Influence of time on crystal attrition in a stirred vessel, *AIChE J.*, **42**, 3554.
Meares, P. (1965). *Polymers: Structure and Bulk Properties*, Van Nostrand, New York.
Monette, L. and Klein, W. (1992). Spinodal nucleation as a coalescence process, *Phys. Rev. Lett.*, **68**, 2336.
Moriyama, A. and Fujita, S. (2007). Crystal growth of ZnO on Si(1 1 1) by metalorganic vapor phase epitaxy, *J. Cryst. Growth*, **298**, 464.
Muller, R. (1989). The influence of grain size on the overall kinetics of surface-induced glass crystallization, *J. Therm. Anal.*, **35**, 823.
Nienow, A. W. and Conti, R. (1978). Particle abrasion at high solids concentration in stirred vessels, *Chem. Eng. Sci.*, **33**, 1077.
Olson, T. and Hamill, P. (1996). A time-dependent approach to the kinetics of homogeneous nucleation, *J. Chem. Phys.*, **104**, 210.
Pannhorst, W. (1997). Glass ceramics: State-of-the-art, *J. Non-Cryst. Solids*, **219**, 198.
Penrose, O. and Lebowitz, J. L. (1976). Towards a rigorous theory of metastability. In: *Fluctuation Phenomena*, eds. E. W. Montroll and J. L. Lebowitz, North-Holland Pub. Co., Amsterdam.
Peskin, C. S. (1975). *Mathematical Aspects of Heart Physiology*, Courant Institute of Mathematical Sciences, New York.
Piorkowska, E., Galeskia, A., and Haudinb, J.-M. (2006). Critical assessment of overall crystallization kinetics theories and predictions, *Prog. Polym. Sci.*, **31**, 549.
Ploss, R. and Mersmann, A. (1989). New model of the effect of stirring intensity on the rate of secondary nucleation, *Chem. Eng. Technol.*, **12**, 137.
Rabani, E., Reichman, D. R., Geissier, P. L., and Brus, L. E. (2003). Drying-mediated self-assembly of nanoparticles, *Nature*, **426**, 271.
Reif, F. (1965). *Fundamentals of Statistical and Thermal Physics*, McGraw-Hill, New York.
Ryan, A. J., Fairclough, J. A., Terrill, N. J., Olmsted, P. D., and Poon, W. D. (1999). A scattering study of nucleation phenomena in polymer crystallization, *Faraday Discuss.*, **112**, 13.
Sastry, S. (2001). The relationship between fragility, configurational entropy and the potential energy landscape of glass-forming liquids, *Nature (London)*, **409**, 164.
Seinfeld, J. H. and Pandis, S. N. (1997). *Atmospheric Chemistry and Physics: From Air Pollution to Climate Change*, John Wiley, New York.
Smoluchowski, M. von. (1916). Drei Vorträge über Diffusion, Brownsche Molekularbewegung und Koagulation von Kolloidteilchen, *Phys. Z.*,**17**, 557.

Strobl, G. (2006). Crystallization and melting of bulk polymers: New observations, conclusions and a thermodynamic scheme, *Prog. Polym. Sci.*, **31**(4), 398–442.

Strogatz, S. H. (2000). From kuramoto to crawford: Exploring the onset of synchronization in populations of coupled oscillators, *Physica D*, **143**, 1.

Suryanarayana, C. (2002). The structure and properties of nanocrystalline materials: Issues and concerns, *JOM J. Miner. Met. Mater. Soc.*, **54**, 24.

Swihart, M. T. and Carr, R. W. (1998). On the mechanism of homogeneous decomposition of the chlorinated silanes. Chain reactions propagated by divalent silicon species, *J. Phys. Chem. A*, **102**, 1542.

Tomozawa, M. (1971). Liquid phase separation and *crystal nucleation* in Li_2O-SiO_2 *glasses*. In: *Advances in Nucleation and Crystallization in Glasses*, eds. L. L. Hench and S. W. Freiman, American Ceramic Society, Columbus, Ohio.

Ulrich, G. D. (1971). Theory of particle formation and growth in oxide synthesis flames, *Combust. Sci. Technol.*, **4**, 47.

Wagner, C. (1961). Theorie der Alterung von Niederschlaegen durch Umloesen (Ostwald Reifung), *Z. Electrochim.*, **65**, 243.

Walker, J. (1969). Acoustic synchrony: Two mechanisms in the snowy tree cricket, *Science*, **166**, 891.

Walker, K. L., Jardine, R. E., Ring, M. A., and O'Neal, H. E. (1998). Mechanisms and kinetics of the thermal decompositions of trichlorosilane, dichlorosilane, and monochlorosilane, *Int. J. Chem. Kinet.*, **30**, 69.

Winfree, T. (1967). Biological rhythms and the behavior of populations of coupled oscillators, *J. Theor. Biol.*, **16**, 15.

Xia, H. and Zinke-Allmang, M. (1998). Rate equation approach to the late stages of cluster ripening, *Physica A*, **261**, 6.

Xu, H. H. K. and Jahanmir, S. (1999). Scratching and grinding of a machinable glass-ceramic with weak interfaces and rising T-curve, *J. Am. Ceram. Soc.*, **78**, 497.

Xu, X. J., Ray, C. S., and Day, D. E. (1991). Nucleation and crystallization of $Na_2O{\cdot}2CaO{\cdot}3SiO_2$ glass by differential thermal analysis, *J. Am. Ceram. Soc.*, **74**, 909.

Yang, J., McCoy, B. J., and Madras, G. (2005a). Temperature effects for isothermal polymer crystallization kinetics, *J. Chem. Phys.*, **122**, 244905.

Yang, J., McCoy, B. J., and Madras, G. (2005b). Kinetics of nonisothermal polymer crystallization, *J. Phys. Chem., B*, **109**, 18550.

Yang, J., McCoy, B. J., and Madras, G. (2006a). A distribution kinetics approach for crystallization of polymer blends, *J. Phys. Chem., B*, **110**, 15198.

Yang, J., McCoy, B. J., and Madras, G. (2006b). Cluster kinetics and dynamics during spinodal decomposition, *J. Chem. Phys.*, **124**, 024713.

Yu, L. (2003). Nucleation of one polymorph by another, *J. Am. Chem. Soc.*, **125**, 6380.

Yu, Z. Q., Tan, R. B. H., and Chow, P. S. (2005). Effects of operating conditions on agglomeration and habit of paracetamol crystals in anti-solvent crystallization, *J. Cryst. Growth*, **279**, 477.

Zachariah, M. R. and Tsang, W. (1995). Theoretical calculation of thermochemistry, energetics, and kinetics of high-temperature $Si_xH_yO_z$ reactions, *J. Phys. Chem.*, **99**, 5308.

Zinke-Allmang, M. (1997). Late stage phase separation on surfaces: Diffusion controlled processes, in: *Surface Diffusion: Atomistic and Collective Processes*, ed. M. C. Tringides, 389–402, Plenum, New York.